A copper(II) chloride coordination compound with 2-phenyl-4,5-dihydro-1H-imidazole ligand: synthesis, characterization, crystal structure, HSA, and DFT studies

Hadi Kargar, Mehdi Fallah-Mehrjardi, Necmi Dege, Muhammad Ashfaq, Khurram Shahzad Munawar, Muhammad Nawaz Tahir, Mahdieh Asgari Bajgirani, Mehdi Sahihi

A copper(II) chloride coordination compound with 2-phenyl-4,5-dihydro-1*H*-imidazole ligand: synthesis, characterization, crystal structure, HSA, and DFT studies

Hadi Kargar[1] · Mehdi Fallah-Mehrjardi[1] · Necmi Dege[2] · Muhammad Ashfaq[3] · Khurram Shahzad Munawar[4,5] · Muhammad Nawaz Tahir[4] · Mahdieh Asgari Bajgirani[6] · Mehdi Sahihi[7]

Abstract

Under ultrasound irradiation in an ethanol solvent, a new coordination complex of Cu(II) was successfully synthesized within a 10-min timeframe through the treatment of an imidazole-based ligand (PDI) with a copper-containing salt. The formation of the complex was verified through elemental (CHN) analysis and FT-IR spectroscopy. Additionally, the supramolecular assembly and packing of atoms in the crystalline units of the copper complex were elucidated using single-crystal X-ray diffraction method. The synthesized compound exhibits an ionic nature, featuring a copper(II) cation inside the coordination sphere and a chloride anion outside of the coordination sphere. The coordination environment around the copper cation is achieved through the bonding of the N-atom of the non-protonated PDI ligands and a chloride ion. To maintain a neutral charge, a second chloride ion serves as a counterion. The bond angles surrounding the Cu(II) ion showed a somewhat deformed square planar geometry of the complex. The non-covalent intermolecular interactions were executed by Hirshfeld surface analysis (HSA), while the theoretical studies were conducted using DFT employing the B3LYP/Def2-TZVP level of theory. The consistency between the theoretical findings and experimental data attested to the reliability of the theoretical conclusions.

Keywords Imidazole ligand · Copper(II) complex · Structure · Hirshfeld · Theoretical studies

✉ Hadi Kargar
h.kargar@ardakan.ac.ir

[1] Department of Chemical Engineering, Faculty of Engineering, Ardakan University, P.O. Box 184, Ardakan, Iran

Introduction

There is immense scientific consideration in the area of imidazoline derivatives. Imidazolines are five-membered N-heterocycles produced from imidazoles by the partial reduction method and can be used as nitrogenous electron donors in organic dyes [1], as catalysts, chiral auxiliaries, and asymmetric catalysis ligands [2–4].

Many imidazolines are biologically active and could be identified in natural organic compounds like topsentines or spongotines extracted from sponges found in the ocean [5]. Because of their anticancer, antiviral, and anti-inflammatory properties, these alkaloids were appealing for biological applications [6]. Clonidine, which contains imidazoline, is utilized in high blood pressure therapeutics. It has been predicted that imidazolines have a role in the treatment of mental disorders and neurodegenerative diseases [7, 8]. Imidazoline and its derivatives are key types of inhibitors that may efficiently prevent CO_2 and H_2S corrosion in carbon steel [9, 10].

Table 1 Crystal data and structural refinements for **[CuCl(PDI)$_3$]Cl** complex

Chemical formula	$C_{27}H_{30}Cl_2CuN_6$
Formula weight	573.02
Temperature (K)	293

[1] Department of Chemistry, Payame Noor University (PNU), Tehran 19395-4697, Iran

[2] Department of Physics, Faculty of Arts and Sciences, Ondokuz Mayıs University, 55139 Samsun, Turkey

[3] Department of Physics, University of Sargodha, Sargodha 40100, Pakistan

[4] Institute of Chemistry, University of Sargodha, Sargodha 40100, Pakistan

[5] Department of Chemistry, University of Mianwali, Mianwali 42200, Pakistan

[6] Department of Physical Chemistry, Faculty of Chemistry, Lorestan University, Lorestan, Iran

[7] Institut de Chimie de Clermont-Ferrand, Université Clermont Auvergne, CNRS, Clermont Auvergne INP, 63000 Clermont-Ferrand, France

Wavelength (Å)	0.71073
Crystal system	Triclinic
Space group *P* 1 *a (Å)* 8.4236(8) *b (Å)* 10.8041(11) *c (Å)* 14.9723(17) *α (°)* 86.829(9) *β (°)* 88.130(9) *γ (°)* 88.151(8)	
Volume (Å^3)	1359.2(2)
Z 2 Radiation type Mo *Kα*	
μ (mm^{-1})	1.03
Crystal size (mm)	0.38 × 0.23 × 0.12
No. of measured, independent, and observed [$I > 2s(I)$] reflections	5030, 5030, 3357
R_{int}	0.121
$(\sin \theta/\lambda)_{max}$ (Å^{-1})	0.606
$R[F^2 > 2\sigma(F^2)]$, $wR(F^2)$, S	0.124, 0.259, 1.25
No. of reflections	5030
No. of parameters	290
No. of restraints	108
H-atom treatment	H-atom parameters constrained
$\Delta\rho_{max}$, $\Delta\rho_{min}$ (e Å^{-3})	0.80, − 0.52

supramolecular assemblies may be achieved by hydrogen bonding [16–18].

With a combination of medicinal qualities and intriguing spectroscopic, magnetic, and structural characteristics, transition metal complexes based on imidazoles and their respective derivatives have received a lot of attention. The complexes of cobalt, nickel, copper, and zinc, for example, have been employed as efficient antibacterial agents [19, 20]. The antifungal actions have also been found for Zn and Ag complexes [21, 22].

Copper is an important element with biological relevance and exhibits a high degree of coordination versatility [23, 24]. It displays structural variation in coordination geometries and the number of imidazole units attached to it [25, 26]. Coordination chemistry based on copper(II)imidazole has been useful in development and production of metal organic hybrids consisting of N,N′ donor ligands and carboxylates [27]. The majority of the reports documented earlier are focused on Cu^{2+} complexes of unsubstituted imidazoles, and N and alkyl substituted imidazoles, while the derivatives other than these have received very little attention [28].

Keeping in mind the above-mentioned properties and on the basis of our previous investigation on the chemistry of copper complexes [29–37], we are reporting the synthesis and structural characteristics of a new Cu^{2+} chlorido

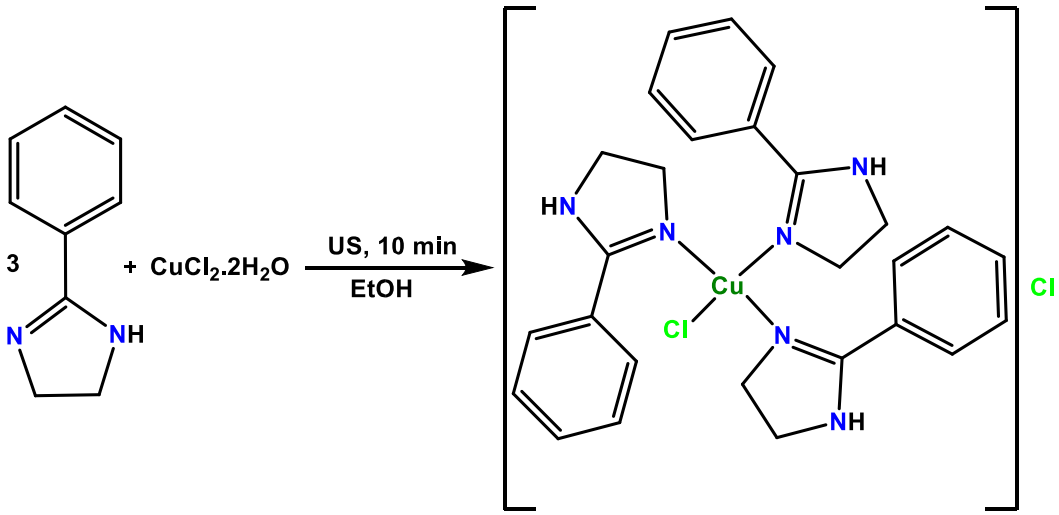

Scheme 1. Synthesis of **[CuCl(PDI)$_3$]Cl** complex under ultrasound irradiation

For many years, researchers have been interested in the study of imidazole derivatives as complexing agents, primarily because imidazole is engaged in essential biological functions [11, 12]. An imidazole molecule has two N atoms; deprotonated N-atom acts as a donor site for metal ion coordination, and several molecules derived from imidazole and other transition metals have already been described [13–15], while the protonated N-atom, on the other hand, is an excellent hydrogen bonding donor, and multidimensional

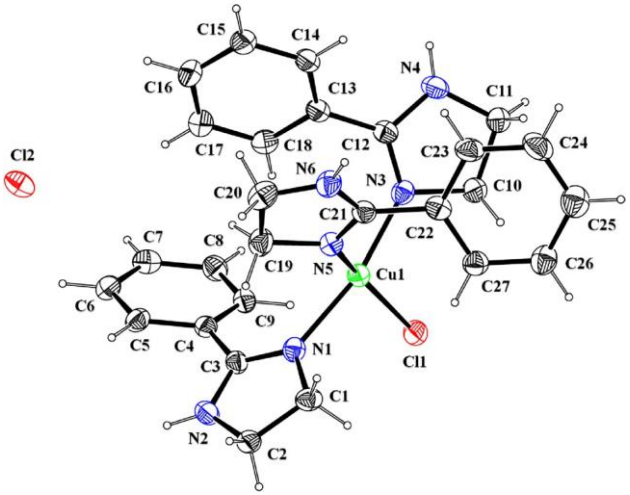

Fig. 1 ORTEP diagram of **[CuCl(PDI)$_3$]Cl** drawn at a 20% probability level. H-atoms can be identified by compact balls of random radii

Table 2 Important bond distances (Å) and bond angles (°) of **[CuCl(PDI)$_3$]Cl**

Bond distances		Bond angles	
Cu1–N5	1.990 (11)	N3–Cu1–N1	166.1 (4)
Cu1–N3	1.955 (10)	N3–Cu1–N5	93.5 (4)
Cu1–N1	2.013 (10)	N5–Cu1–N1	87.3 (4)
Cu1–Cl1	2.286 (3)	N3–Cu1–Cl1	92.9 (3)
N1–C3	1.297 (13)	N5–Cu1–Cl1	158.8 (3)
N1–C1	1.491 (14)	N1–Cu1–Cl1	91.2 (3)

complex using 2-phenyl-4,5-dihydro-1*H*-imidazole (PDI) as a ligand. We have characterized the synthesized complex by elemental (CHN), FT-IR, and SC-XRD and conducted theoretical studies to explore further understandings of spectroscopic and supramolecular aspects.

Experimental

Materials and methods

Various solvents and chemicals utilized in the present investigation are of experimental quality and were acquired from Sigma-Aldrich. The CHN study of ligand and its associated complex with copper was conducted via a Heraeus CHN-OFLASH EA 1112 device. The stretching vibrational evaluation of synthesized species has been recorded using infrared light by the IRPrestige-21 spectrophotometer. A UP 400S ultrasonic processor having a 3-mm broad and 140-mm long probe which was inserted in a mixture of reacting precursors

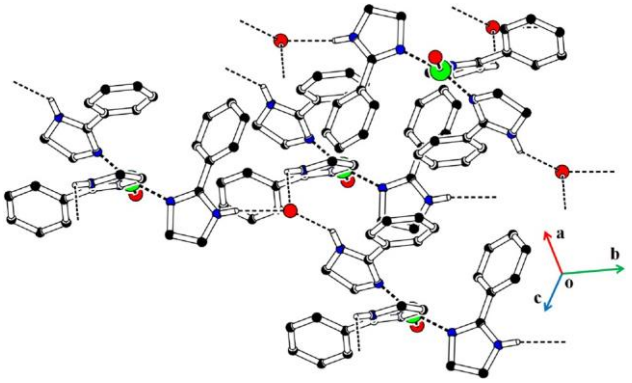

Fig. 2 Packing illustration showing H-bonding interactions linking cations and anions

Table 3 Hydrogen bond geometry (Å, °)

D–H···*A*	*D*–H	H···*A*	*D*···*A*	< (*D*–H···*A*°)
N2–H2···Cl2^{i}	0.86	2.45	3.198 (11)	146
N4–H4···Cl2^{ii}	0.86	2.53	3.247 (10)	141
N6–H6*A*···Cl2^{iii}	0.86	2.66	3.149 (13)	117

Symmetry codes: (i) $-x+1, -y, -z+1$; (ii) $-x, -y+1, -z+1$; (iii) $-x+1, -y+1, -z+1$

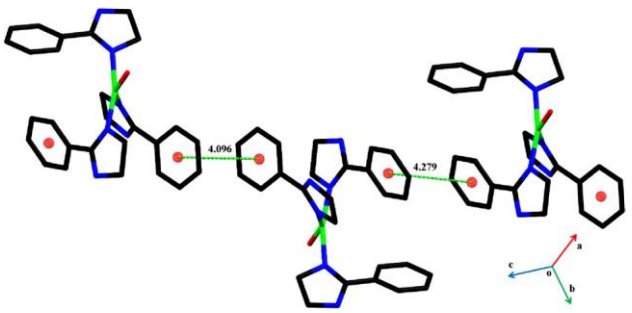

Fig. 3 The pictorial layout of off-set π ··· π stacking interactions. Distances are measured in Å

was utilized for sonication. The ultrasonication took place at 25 °C in a 40-cm^3 glass chamber.

Synthesis of [CuCl(PDI)$_3$]Cl complex

An ethanolic (15 mL) solution of the PDI (1.5 mmol, 0.219 g) was added to an aqueous (15 mL) $CuCl_2.2H_2O$ (0.5 mmol, 0.085 g) solution and ultrasonicated for 10 min. The resultant green liquid underwent filtering to remove unwanted solid particles before it was let for evaporation at 25 °C. After several days, green cubic crystals of complex appropriate for X-ray analysis were formed. **[CuCl(PDI)$_3$]Cl**: Yield 73%. Anal. Calc. for $C_{27}H_{30}Cl_2CuN_6$: C, 56.59; H, 5.28; N, 14.67%, Found: C,

56.47; H, 5.32; N, 14.55%. FT-IR (KBr, c m^{-1}): 3105 (ν_{N-H}); 1604 ($\nu_{C=N}$); 1562, 1473 ($\nu_{C=C}$).

Particulars of X-ray structure solutions and refinement

A crystal of proper dimensions was fixed on Bruker Kappa Apex-II CCD diffractometer having APEX-II software for data collection. Structural solutions and refinements were executed on SHELXT-2014 [38] and SHELXL 2019/2 [39],

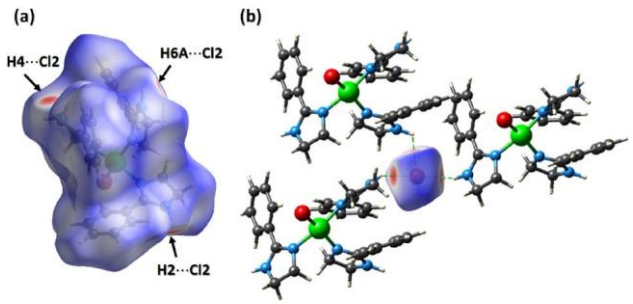

Fig. 4 HS plotted over d_{norm} for **a** cation, and **b** chloride anion

correspondingly. The heavier atoms like Cu, Cl, C, and N were allotted with anisotropic displacement parameters; however, H-atoms were allotted isotropic displacement parameters. The H-atoms were positioned through a riding model. PLATON [40] is used for structural validation as well as for making ORTEP and packing diagrams. Mercury 4.0 [41] was also used for graphical purposes. Table 1 describes the crystal data and refinement statistics of **[CuCl(PDI)$_3$] Cl** complex.

Computational details

The Gaussian 09 software has been employed to perform the theoretical computations [42], while B3LYP functional utilizing a Def2-TZVP basis set was applied for optimization of geometry of copper complex. Frequency analysis was conducted to validate that the complex structure resides in the most energetically favorable state on the molecular potential energy surface (PES), thereby confirming its stability. The electronic density of state (DOS) of complex, which represents the electrical characteristics, was acquired using a GaussSum program [43]. The energy gap (E_{gap}) was measured based on the following equation: $E_{gap} = E_{LUMO} - E_{HOMO}$, where E_{HOMO} and E_{LUMO} are related to the energies of the highest occupied molecular orbital (HOMO) and the lowest

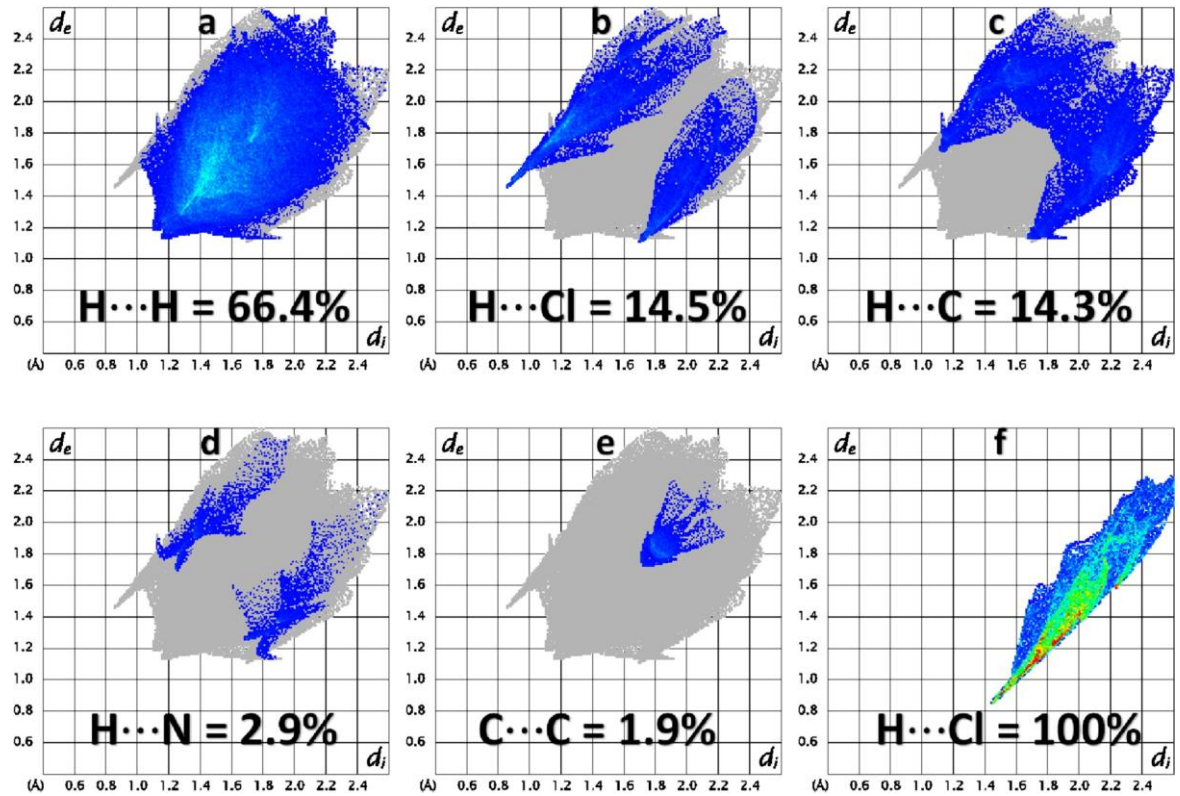

Fig. 5 2D plots by using the surface of cation (**a–e**) and chloride anion (**f**)

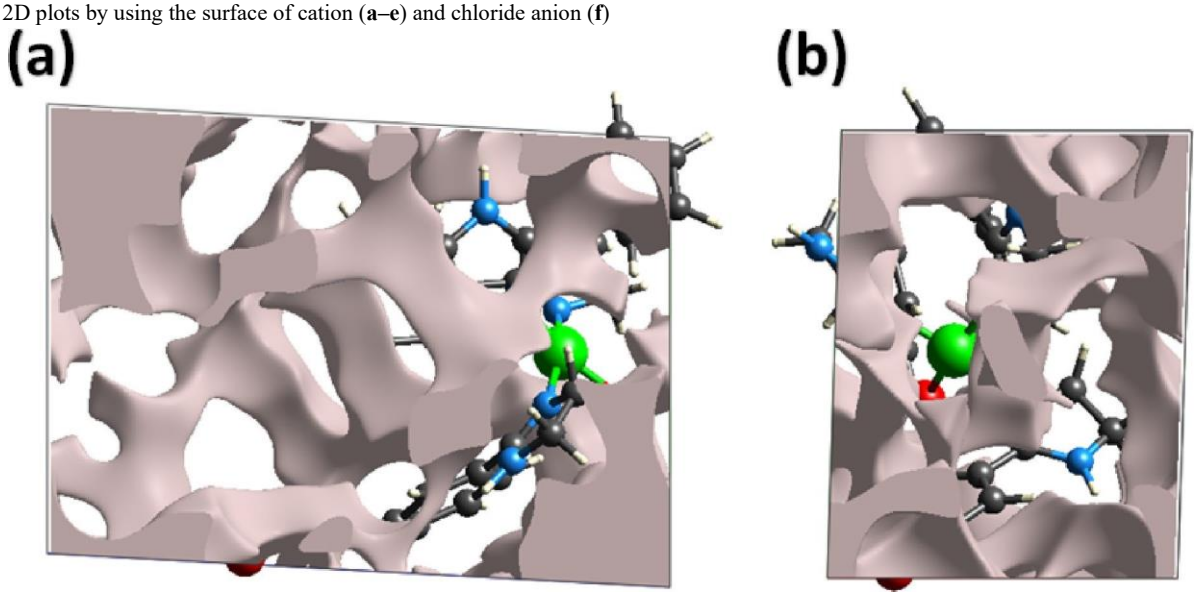

Fig. 6 Graphical representation of voids in **a** *a*-axis, **b** *c*-axis

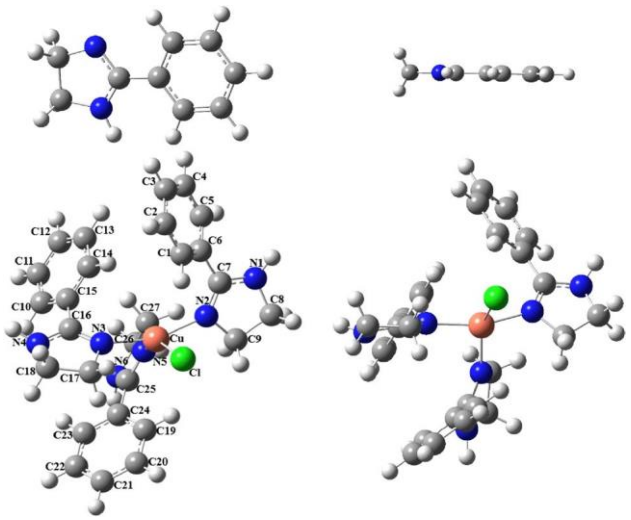

Fig. 7 The top and side views of the geometry optimized structures of complex and ligand in vacuum using B3LYP/Def2-TZVP method. The H-atoms attached to carbon rings (gray) are shown with small white spheres, chlorine atoms in green, nitrogen atoms in blue, and copper atom in pink

unoccupied molecular orbital (LUMO), correspondingly. The contour plots of HOMO and LUMO were also created by means of the GaussView package [44]. Finally, the obtained molecular electrostatic potential (MEP) outputs were taken into consideration for natural bond orbital (NBO) computations.

Results and discussion

Synthesis

The **[CuCl(PDI)$_3$]Cl** complex was produced by reacting 2-phenyl-4,5-dihydro-1*H*-imidazole (PDI) ligand with copper(II) chloride dihydrate in ethanol under ultrasonic irradiation for a period of 10 min (Scheme 1).

Crystal structure analysis

The crystal structure of **[CuCl(PDI)$_3$]Cl** complex is ionic with a copper(II) containing cation and chloride anion. The coordination sphere around copper is completed by N-atom of three non-protonated PDI ligands and a chloride ion. The second chloride ion acts as a counter ion to make the structure neutral. Cu–N bond distances vary from 1.990 (11) to 2.013 (10) Å, whereas Cu–Cl bond length is 2.286 (3) Å. Bond angles vary from 87.3 (4) to 166.1 (4)° (Fig. 1, Table 2). The structural parameter for a compound is 0.12 showing that coordination geometry is slightly distorted square planar. The dihedral angle concerning 4,5-dihydro-1*H*-imidazole ring A (C1-C3/N1/ N2) and phenyl ring B (C4–C9) is 31.7 (5)° in the first PDI ligand, whereas the dihedral angle between the corresponding rings in second and third PDI ligands is 36.4 (6)° and 39.6 (5)°, respectively. The 4,5-dihydro-1*H*-imidazole ring of PDI second and third ligand adopted twisted conformation on C10–C11 bond and envelope conformation on C19-atom, respectively. The cations are linked with anions by the use of N–H$^{\cdots}$ Cl bonding. The NH group of each PDI ligand acts as a H-bond donor but each NH group

Table 4 Selected bond lengths (Å) and angles (degree) of the complex in gas phase (compared to the experimental values)

Bond length	Cal	Exp	Bond length	Cal	Exp	Bond angle	Cal	Exp
Cu–Cl 2.27477	2.28588	C15–C16 1.47517	1.47712	Cl–Cu–N2 89.74132		Cu–N2 2.02339	2.01313	C16–N3 1.29869	1.29261	C9–C24 1.47788
95.07436	92.88003	Cu–N3 2.02258	1.95526	N3–C17 1.48484	1.51729	Cl–Cu–N5 143.91692	158.81851	Cu–N5 2.06775	1.99053	C17–C18
1.54125	1.53817	N5–Cu–N2 91.92951	87.32376	C1–C2 1.38960	1.38956	C18–N4 1.46734	1.45111	N5–Cu–N3 97.05982	93.53044	C2–C3
1.39087	1.39065	N4–C16 1.35947	1.36516	Cl6–N3–Cu 130.56877	131.25911	C3–C4 1.39130	1.39015	C19–C20 1.38825	1.38966	C25–N5–
Cu 129.39552	131.25508	C4–C5 1.38857	1.38956	C20–C21 1.39058	1.38938	C7–N2–Cu 132.83866	133.57146			
C5–C6	1.39839	1.39022	C21–C22 1.39131	1.39024	C6–C7–N2	126.17523	125.36303	C6–C7	1.47529	
	1.46315	C22–C23 1.38770	1.38922	C15–C16–N3	126.37917	124.44415				
C7–N1	1.36083	1.37318	C23–C24 1.39989	1.38996	C24–C25–N5	126.21752	122.27055	N1–C8	1.46708	
	1.39077	C24–C25 1.47306	1.51166	N1–C7–N2	114.23720	110.56948				
C8–C9	1.54630	1.49258	C25–N6	1.36252	1.33053	N3–C16–N4	114.45135	114.42648		
C9–N2	1.47772	1.49135	N6–C26	1.46551	1.38360	N5–C25–N6	114.19013	117.24074		
N2–C7	1.29611	1.29702	C26–C27 1.54243	1.53734	C10–C11	1.38863	1.39056			
	C27–N5	1.47929	1.49826							
C11–C12	1.39139	1.39021	N5–C25	1.30021	1.32190					
C12–C13	1.39068	1.38958								
C13–C14	1.38941	1.39055								

C14–C15	1.39609	1.38912	

form H-bond with the unique symmetry related chloride ion, as a result, a 2D network is formed in (001) with base vectors [100] and [010] (Fig. 2, Table 3). N-atom and chloride of the cation do not take part in H-bonding interaction as a consequence, cations are not connected via any sort of H-bonding. The supramolecular assembly is furthermore strengthened by off-set $\pi \cdots \pi$ stacking interfaces between phenyl rings with ring off-set varying from 2.028 to 2.522 Å (Fig. 3). All the intratomic contacts and intermolecular contacts with distance less than 4 Å are given in Tables S1 whereas crystal structure and S2, respectively. Only one crystal structure is found in the literature in which 2-phenyl-4,5-dihydro-1*H*-imidazole acts as a ligand that is for the palladium with CSD reference code JOJPEE [45]. But coordination geometry of JOJPEE is different from coordination geometry of compound as the in JOJPEE, the palladium center is coordinated by two PDI ligands and one chloride ion. The other difference is that crystal structure of JOJPEE is non-ionic, of our compound is ionic.

Fig. 8 Bond lengths for the ligand (**a**), and complex in the gas phase (**b**)

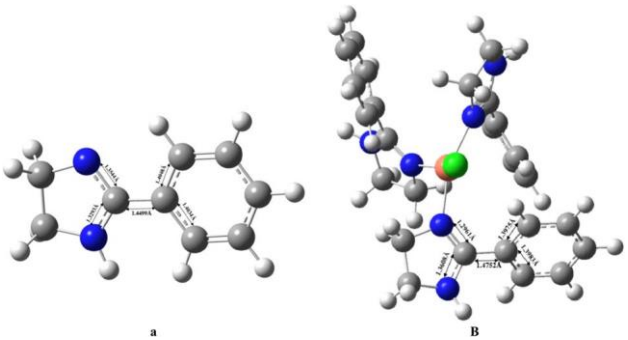

Table 5 The experimental and calculated IR stretching vibrational bands (cm^{-1}) as well as relative errors of complex

Assignment	Cu Complex		
	Exp	Calc	Relative error (%)[a]
ν_{N-H}	3105	3607	16.16
$\nu_{C=N}$	1605	1605	0.00
$\nu_{C=C}$	1562	1562	0.00
ν_{C-H}	2978	3201	7.5

[a] Relative error (%) = $(X_{Calc} - X_{Exp}) * 100/X_{Exp}$

Hirshfeld surface analysis

The current era is the era of supramolecular chemistry as the knowledge of supramolecular assemblage like intermolecular interactions, helps to explore the properties of crystal. It encourages researchers working in that field to synthesize novel crystals with better properties than already

HOMO **LUMO**

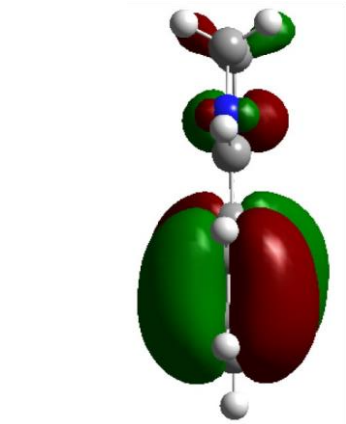
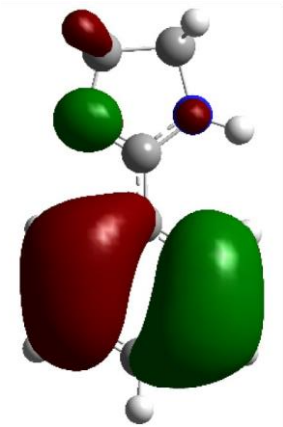
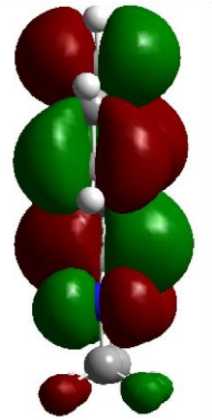
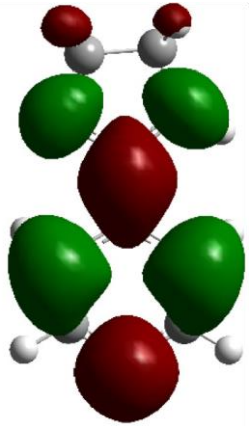
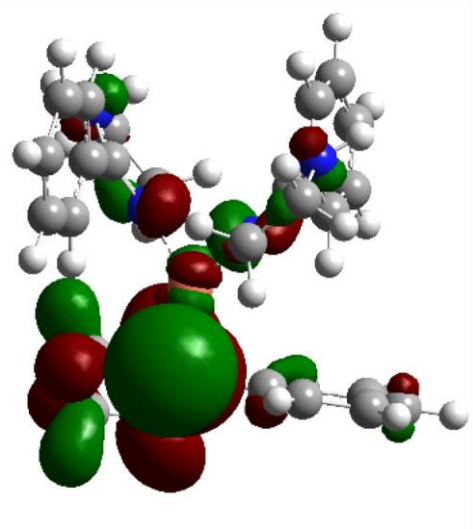
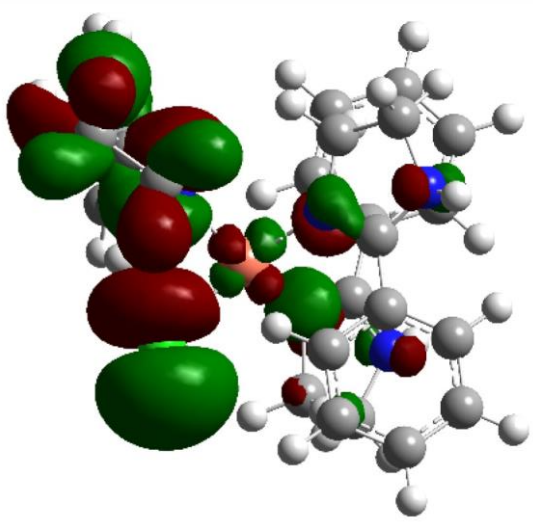
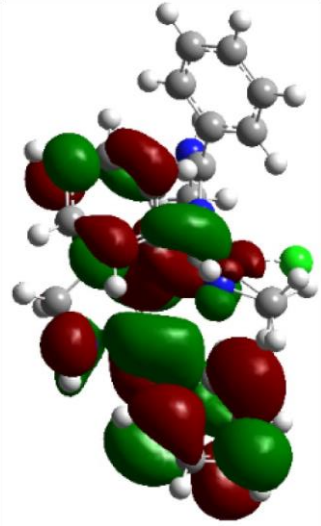
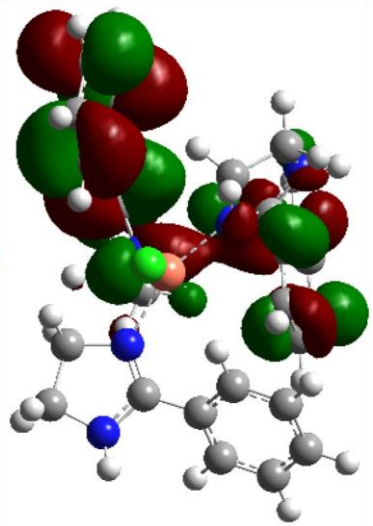

Fig. 9 FMOs of ligand and complex utilizing B3LYP/Def2-TZVP approach

Table 6 Quantum chemical parameters of ligand and complex (energies are reported in eV)[a]

Compound	E_{HOMO}	E_{LUMO}	E_{gap}	I	A	η	S	χ	μ	ω
Ligand	− 8.22	− 3.10	5.12	8.22	3.10	2.56	0.19	5.66	− 5.66	6.25
Complex (gas)	− 9.09	− 4.06	5.03	9.09	4.06	2.52	0.20	6.57	− 6.57	8.59

[a] Ionization potential ($I = -E_{HOMO}$); Electron affinity ($A = -E_{LUMO}$); Softness ($S = 1/2\eta$); Hardness ($\eta = (I–A)/2$); Chemical potential ($\mu = -(I + A)/2$); Electronegativity ($\chi = (I + A)/2$); Electrophilicity ($\omega = \mu^2/2\eta$)

known crystals. The analysis that is widely used nowadays for inspection of intermolecular interactions is HSA. We performed that analysis by utilizing Crystal Explorer version 21.5 [46]. Normalized distances-based Hirshfeld surface is used to identify short contacts in crystals [47, 48]. In present case, as expected, each cation is surrounded by chloride anions and each chloride anion is surrounding by cations. To be precise, each cation is surrounded by three chloride ions as can be perceived in Figs. 4a and b and the short contacts are displayed in Fig. 4.

The depiction of overall interactions can be done by 2D fingerprint plots. 2D plots make use of Hirshfeld surface [49, 50]. The surface of cation and chloride anion provides five and one 2D plots, respectively. H ⋯ H contact is the most important one with the contribution of 66.4% in supramolecular assembly stabilization, followed by H ⋯Cl, H ⋯ C, H ⋯ N, and C ⋯ C. The chloride anion interacts with only H-atoms of the neighboring cations (Fig. 5).

A crystal with smaller voids is the gesture for its good ability to react whenever some sort of stress is imposed. The idea of summing up the electron density is used for void's calculations [51, 52]. Voids are shown in Fig. 6. The volume of voids is 169.79 $Å^3$ with 12.5% space occupation in the unit cell. As maximum space is filled by molecules in the unit cell indicating that the crystal will have good mechanical response.

Theoretical investigation

The optimized structural analysis

To investigate the prepared compound, we optimize their structures through theoretical calculations using B3LYP/Def2-TZVP. This approach facilitates the determination of both the lowest energy and the most stable structure. Additionally, all analysis calculations exhibit zero hypothetical frequencies, indicating that the optimal set resides at the lowest point of local energy. Figure 7 presents the ligand and complex geometry optimized structures, while Table 4 provides selected bond distances and bond angles of **[CuCl(PDI)$_3$]Cl** in the gas phase. Geometrical comparisons between the theoretically optimized and experimentally determined structures reveal a strong agreement between them. Any minor discrepancies are likely attributed to experimental outcomes obtained from solid state molecules; however, the optimization process occurred in the gas phase. In the optimal ligand structure, C=N bond length measures 1.33 Å, while its corresponding average value in the complex structure (gas phase) is approximately 1.36 Å. The observed increase in C=N bond length (as shown in Fig. 8), further supports the notion that it is a consequence of complex formation.

Dihedral angle analysis of the ligand shows that the angle between N=C–C=C is about 1° and nearly flat, while this dihedral angle in the gas phase is approximately 48.109°. As a result, the ligand takes a non-planar structure in the complex structure.

FT-IR study

By comparing the vibrational-stretching frequencies calculated for the complex and the obtained experimental values, the stretching frequencies of N–H and C-H were increased, while the stretching frequencies of C=C and C=N remain almost constant (Table 5). This comparison shows a very good agreement, and only in the case of N–H stretching vibration is observed a difference of about 16.16%, which may be due to the solvent effects**.** While the infrared spectrum was measured on the crystals, it is important to consider that even in crystal structures, solvent molecules can be present in the crystal lattice through coordination or inclusion. In such cases, the interaction between the solvent molecules and the complex can affect the vibrational frequencies. Additionally, solvent molecules may influence the crystal packing and the local environment of specific functional groups. Our suggestion of solvent effects influencing the N–H vibrational mode is based on the understanding that solvent molecules can interact with the complex in its crystalline form, leading to changes in vibrational frequencies. The hydrogen bonding behavior of the N–H group can indeed be precisely known in the crystal, but the presence of solvent molecules may introduce additional vibrational modes or alter the energy landscape of existing modes. We acknowledge that the solvent effect is a complex phenomenon and can manifest in various ways,

even in crystalline structures. This solvent effect is neglected in calculations, could leading to differences between calculated and experimental frequencies.

Softer molecules display enhanced polarizability since they require less energy to bridge energy gap and for the excitation of an electron from HOMO to LUMO [54]. The

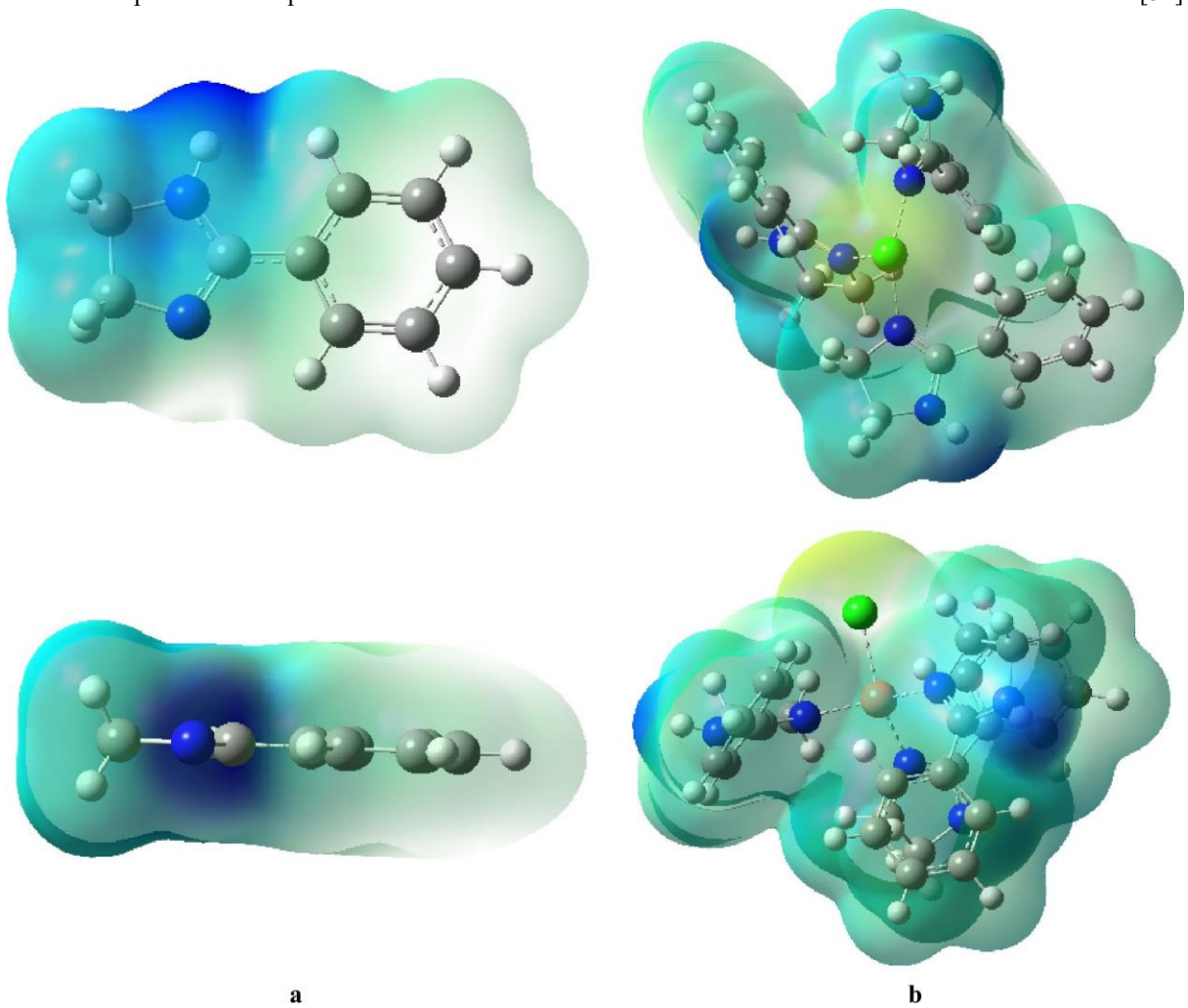

Fig. 10 MEP maps for the ligand (**a**) and Cu complex in the gas phase (**b**) to be calculated at the B3LYP/Def2-TZVP (− 0.04 to + 0.04 a.u.). The yellow, blue, and green colors indicate negative, positive, and neutral electrostatic areas, respectively

Frontier molecular orbitals (FMOs), molecular electrostatic potential (MEP) maps, and natural bond orbital (NBO) analyses

FMO exploration of the studied compounds assists in illustrating their kinetic stability and reactivity in chemical processes [53]. The shapes of calculated HOMO and LUMO orbitals of complex show that HOMO orbital is located both on copper metal, chlorine, and ligand, whereas LUMO orbital is mainly sited on ligand (Fig. 9). This point can cause the charge transfer from ligand to metal. The quantum chemical descriptors of ligand and complex are recorded in Table 6.

Considering the information provided in Table 6, the Cu complex exhibits a narrower energy gap in gas phase (5.03 eV) relative to ligand (5.12 eV), indicating its softer nature. compounds exhibit consistent outcomes in terms of chemical hardness and softness. The chemical potential values (− 5.66, and − 6.27 eV for the ligand and complex, respectively) suggest that compounds are stable and unlikely to undergo decomposition to their components. Additionally, the electrophilicity index data of complex demonstrate its greater electrophilic strength in the gas phase when compared to the ligand [55]. The observed differences in electrophilicity index values between ligand and complex could be due to the formation of complex.

MEP map serves as a beneficial and significant analysis in elucidating nucleophilic and electrophilic characteristics of compounds. It provides insights into shape, size, and electrostatic dispersal of a compound, making it a valued parameter for exploring structural interactions and photochemical features of a compound [56]. Within the

complex, the central position is occupied by the copper ion, which

Table 7 Summary of NAC, NP, and NEC analyses of Cu complex by the B3LYP approach with Def2-TZVP basis set

Atom	NACs	NPs				NECs
		Core				
	Valence			Rydberg	Total	
Cu	0.91732	17.99639	10.07316	0.01313	28.08268	[core]4S$^{(0.32)}$3d$^{(9.35)}$4p$^{(0.40)}$
Cl	− 0.62844	9.99982	7.62201	0.00660	17.62844	[core]3S$^{(1.93)}$3p$^{(5.69)}$
N1	− 0.51987	1.99927	5.48264	0.03795	7.51987	[core]2S$^{(1.35)}$2p$^{(4.13)}$3p$^{(0.02)}$3d$^{(0.01)}$
N2	− 0.55666	1.99942	5.53448	0.02277	7.55666	[core]2S$^{(1.29)}$2p$^{(4.25)}$3p$^{(0.01)}$3d$^{(0.01)}$
N3	− 0.53116	1.99929	5.49568	0.03619	7.53116	[core]2S$^{(1.36)}$2p$^{(4.14)}$3p$^{(0.02)}$3d$^{(0.01)}$
N4	− 0.54557	1.99941	5.52387	0.02228	7.54557	[core]2S$^{(1.28)}$2p$^{(4.24)}$3p$^{(0.01)}$3d$^{(0.01)}$
N5	− 0.53249	1.99929	5.49748	0.03572	7.53249	[core]2S$^{(1.36)}$2p$^{(4.14)}$3p$^{(0.02)}$3d$^{(0.01)}$
N6	− 0.55022	1.99941	5.52829	0.02252	7.55022	[core]2S$^{(1.28)}$2p$^{(4.24)}$3p$^{(0.01)}$3d$^{(0.01)}$
C1	− 0.23147	1.99941	4.21772	0.01433	6.23147	[core]2S$^{(1.05)}$2p$^{(3.17)}$
C2	− 0.22388	1.99942	4.21115	0.01331	6.22388	[core]2S$^{(1.05)}$2p$^{(3.16)}$
C3	0.46159	1.99921	3.51419	0.02501	5.53841	[core]2S$^{(0.83)}$2p$^{(2.68)}$3p$^{(0.01)}$
C4	− 0.11690	1.99898	4.09677	0.02115	6.11690	[core]2S$^{(0.91)}$2p$^{(3.18)}$3p$^{(0.01)}$
C5	− 0.17975	1.99912	4.16217	0.01845	6.17975	[core]2S$^{(0.97)}$2p$^{(3.19)}$3p$^{(0.01)}$3d$^{(0.01)}$
C6	− 0.20237	1.99920	4.18389	0.01929	6.20237	[core]2S$^{(0.98)}$2p$^{(3.21)}$3p$^{(0.01)}$
C7	− 0.18741	1.99919	4.16941	0.01882	6.18741	[core]2S$^{(0.98)}$2p$^{(3.19)}$3p$^{(0.01)}$
C8	− 0.20225	1.99919	4.18420	0.01886	6.20225	[core]2S$^{(0.98)}$2p$^{(3.21)}$3p$^{(0.01)}$
C9	− 0.18492	1.99910	4.16760	0.01822	6.18492	[core]2S$^{(0.98)}$2p$^{(3.19)}$3p$^{(0.01)}$3d$^{(0.01)}$
C10	− 0.23190	1.99940	4.21756	0.01494	6.23190	[core]2S$^{(1.05)}$2p$^{(3.17)}$3p$^{(0.01)}$
C11	− 0.22578	1.99942	4.21316	0.01321	6.22578	[core]2S$^{(1.05)}$2p$^{(3.16)}$
C12	0.46564	1.99921	3.51014	0.02501	5.53436	[core]2S$^{(0.83)}$2p$^{(2.68)}$3p$^{(0.01)}$
C13	− 0.11382	1.99897	4.09383	0.02103	6.11382	[core]2S$^{(0.91)}$2p$^{(3.18)}$3p$^{(0.01)}$
C14	− 0.18187	1.99912	4.16422	0.01853	6.18187	[core]2S$^{(0.97)}$2p$^{(3.19)}$3p$^{(0.01)}$3d$^{(0.01)}$
C15	− 0.20054	1.99920	4.18219	0.01915	6.20054	[core]2S$^{(0.98)}$2p$^{(3.20)}$3p$^{(0.01)}$
C16	− 0.18983	1.99919	4.17188	0.01876	6.18983	[core]2S$^{(0.98)}$2p$^{(3.19)}$3p$^{(0.01)}$
C17	− 0.20135	1.99919	4.18367	0.01849	6.20135	[core]2S$^{(0.98)}$2p$^{(3.20)}$3p$^{(0.01)}$
C18	− 0.18337	1.99908	4.16621	0.01808	6.18337	[core]2S$^{(0.97)}$2p$^{(3.19)}$3p$^{(0.01)}$3d$^{(0.01)}$
C19	− 0.23289	1.99941	4.21778	0.01569	6.23289	[core]2S$^{(1.05)}$2p$^{(3.17)}$3p$^{(0.01)}$
C20	− 0.22303	1.99942	4.20995	0.01366	6.22303	[core]2S$^{(1.05)}$2p$^{(3.16)}$3d$^{(0.01)}$
C21	0.46479	1.99921	3.51053	0.02547	5.53521	[core]2S$^{(0.83)}$2p$^{(2.68)}$3p$^{(0.01)}$
C22	− 0.11933	1.99897	4.09904	0.02132	6.11933	[core]2S$^{(0.91)}$2p$^{(3.19)}$3p$^{(0.01)}$
C23	− 0.17968	1.99912	4.16198	0.01857	6.17968	[core]2S$^{(0.97)}$2p$^{(3.19)}$3p$^{(0.01)}$3d$^{(0.01)}$
C24	− 0.20078	1.99920	4.18243	0.01916	6.20078	[core]2S$^{(0.98)}$2p$^{(3.20)}$3p$^{(0.01)}$
C25	− 0.18481	1.99919	4.16686	0.01875	6.18481	[core]2S$^{(0.98)}$2p$^{(3.18)}$3p$^{(0.01)}$
C26	− 0.19926	1.99919	4.18090	0.01916	6.19926	[core]2S$^{(0.98)}$2p$^{(3.20)}$3p$^{(0.01)}$

resides in a positive electrostatic area distinguishable by its nitrogen atoms to the orbitals of copper. This charge transfer blue color. This region signifies a favorable spot for nucleo- from the ligand to Cu is consistent with the outputs of examphilic attacks, while the majority of negative charges are ining HOMO and LUMO orbitals. The MEP results also concentrated around the chlorine atom (Fig. 10). show a positive charge density on the ligand, which agrees The analysis of NBO is a vital method for examining with the above-mentioned conclusion.
interactions and bonding within and between molecules. It
also serves as the right foundation to inspect charge trans-

fer in the molecular species [57]. Table 7 provides natu- **Conclusion** ral atomic

charges (NACs), natural electron configurations
(NECs), and natural populations (NPs) of Cu, Cl, N, and Herein, we are reporting the synthesis of **[CuCl(PDI)$_3$]Cl** C atoms derived from complex through NBO investiga- complex with 4,5-dihydro-1*H*-imidazole (PDI) ligand is tion. Upon complexation, initial charge of Cu^{2+} decreases, proven to be a significant monodentate ligand. The complex indicating a shift of electronic density from the orbitals of

C27 −0.17429 −0.17429 4.15674 0.01845 6.17429 [core]$2S^{(0.97)}2p^{(3.19)}3p^{(0.01)}3d^{(0.01)}$ shows a sp^2d hybridization to adopt a somewhat distorted square planar coordination geometry, which is supported by respective bond angles around the Cu^{+2} ion acquired from the X-ray data. The FMO analysis was utilized to showcase chemical reactivity and kinetic stability of synthesized compound. The MEP analysis reveals that copper ion within the complex is a highly favorable site for a nucleophilic attack. Additionally, NBO analysis indicates that the charge on Cu^{+2} decreases from its usual value on complexation with ligand.

Appendix 1: Supplementary data

CCDC 2284468 holds supplementary crystallographic data for **[CuCl(PDI)$_3$]Cl**, which can be acquired without any charges through http:// www. ccdc. cam. ac. uk/ conts/ retri eving. html, or from Cambridge Crystallographic Data Centre, 12 Union Road, Cambridge CB2 1EZ, UK; fax: (+ 44) 1223–336-033; or e-mail: deposit@ccdc.cam.ac.uk.

Supplementary Information The online version contains supplementary material available at https:// doi. org/ 10. 1007/ s13738-024- 03016-8.

Acknowledgements Ardakan and Payame Noor University provided practical assistance for our project, which we warmly acknowledged.

Declarations

Conflict of interest The authors indicate that they have no known competing financial interests or personal affiliations that may seem to have impacted the work revealed in this manuscript.

References

1. Y.S. Priya, K.R. Rao, P.V. Chalapathi, A. Veeraiah, J. Mod. Phys. **9**, 753 (2018)
2. T. Isobe, K. Fukuda, Y. Araki, T. Ishikawa, Chem. Commun. (2001). https:// doi. org/ 10. 1039/ b0091 731
3. F. Menges, M. Neuburger, A. Pfaltz, Org. Lett. **4**, 4713 (2002)
4. N.A. Boland, M. Casey, S.J. Hynes, J.W. Matthews, H. MullerBunz, P. Wilkes, Biomol. Chem. **2**, 1995 (2004)
5. S. Tsujii, K.L. Rinehart, Y. Kashman, S.S. Cross, M.S. Lui, S.A. Pomponi, M.C. Diaz, J. Org. Chem. **53**, 5446 (1988)
6. X. Guinchard, Y. Vallee, J.N. Denis, J. Org. Chem. **72**, 3972 (2007)
7. C. Dardonville, I. Rozas, Med. Res. Rev. **24**, 639 (2004)
8. M. Krasavin, Eur. J. Med. Chem. **97**, 525 (2015)
9. L.M. Rodríguez-Valdez, W. Villamisar, M. Casales, J.G. González-Rodriguez, A. Martínez-Villafañe, L. Martinez, D. Glossman-Mitnik, Corros. Sci. **48**, 4053 (2006)
10. C.A. González-Rodríguez, F.J. Rodríguez-Gómez, J. GenescáLlongueras, Electrochim. Acta **54**, 86 (2008)
11. W. Wu, J. Xie, D. Xie, Russian. J. Inorg. Chem. **55**, 384 (2010)
12. P. Mura, A. Casini, G. Marcon, L. Messori, Inorg. Chim. Acta **312**, 74 (2001)
13. N. Masciocchi, G.A. Ardizzoia, S. Brenna, F. Castelli, S. Galli, A. Maspero, A. Sironi, Chem. Commun. (2003). https:// doi. org/ 10. 1039/ b3028 40b
14. F. Lambert, J.P. Renault, C. Policar, I. Morgenstern-Badaraua, M. Cesario, Chem. Commun. (2000). https:// doi. org/ 10. 1039/ a9070 68k
15. X.C. Huang, J.P. Zhang, Y.Y. Lin, X.L. Yu, X.M. Chen, Chem. Commun. (2004). https:// doi. org/ 10. 1039/ b4016 91b
16. A.M. Atria, P. Cortes, M.T. Garland, R. Baggio, Acta Crystallogr. Sect. C **59**, m396 (2003)
17. F.F. Jian, P.S. Zhao, H.L. Xiao, S.S. Zhang, Chin. J. Chem. **20**, 1134 (2002)
18. K.B. Shiu, C.H. Yen, F.L. Liao, S.L. Wang, Acta Crystallogr., Sect. E **59**, m1189 (2003)
19. S.O. Podunavac-Kuzmanović, L.S. Vojinović, Acta Period. Technol. **34**, 119 (2003)
20. S.O. Podunavac-Kuzmanović, V.M. Leovac, G.S. Ćetković, S.L. Markov, Acta Period. Technol. **33**, 151 (2002)
21 . A. Mastrolorenzo, C.T. Supuran, Metal Based Drugs **7**, 49 (2000)
22. A. Mastrolorenzo, A. Scozzafava, C.T. Supuran, J. Enz. Inhib. **15**, 517 (2000)
23. P.M. Utsu, T.E. Gber, D.O. Nwosa, A.D. Nwagu, I. Benjamin, I.J. Ikot, E.A. Eno, O.E. Offiong, A.S. Adeyinka, H. Louis, Polycycl. Aromat. Compd. (2023). https:// doi. org/ 10. 1080/ 10406 638. 2023. 21864 44
24. P. Segľa, J. Pavlik, Inorganics **11**, 250 (2023)
25. A.A. Martinez, C.P. Landee, D.A. Dickie, J.L. Wikaira, F. Xiao, M.M. Turnbull, J. Coord. Chem. **76**, 232 (2023)
26. N.S. Alshehri, A.A. Sharfalddin, D. Domyati, A.S. Basaleh, M.A. Hussien, J. Indian Chem. Soc. **99**, 100692 (2022)
27. S.S. Batool, W.T. Harrison, Q. Syed, M.S. Haider, J. Coord. Chem. **71**, 1380 (2018)
28 . S. Godlewska, J. Jezierska, K. Baranowska, E. Augustin, A. Dołęga, Polyhedron **65**, 288 (2013)
29. H. Kargar, F. Aghaei-Meybodi, R. Behjatmanesh-Ardakani, M.R. Elahifard, V. Torabi, M. Fallah-Mehrjardi, M.N. Tahir, M. Ashfaq, K.S. Munawar, J. Mol. Struct. **1230**, 129908 (2021)
30. H. Kargar, F. Aghaei-Meybodi, M.R. Elahifard, M.N. Tahir, M. Ashfaq, K.S. Munawar, J. Coord. Chem. **74**, 1534 (2021)
31. H. Kargar, A.A. Ardakani, M.N. Tahir, M. Ashfaq, K.S. Munawar, J. Mol. Struct. **1233**, 130112 (2021)
32. H. Kargar, A.A. Ardakani, K.S. Munawar, M. Ashfaq, M.N. Tahir, J. Iran. Chem. Soc. **18**, 2493 (2021)
33. H. Kargar, A.A. Ardakani, M.N. Tahir, M. Ashfaq, K.S. Munawar, J. Mol. Struct. **1229**, 129842 (2021)
34. H. Kargar, R. Behjatmanesh-Ardakani, V. Torabi, M. Kashani, Z. Chavoshpour-Natanzi, Z. Kazemi, V. Mirkhani, A. Sahraei, M.N. Tahir, M. Ashfaq, K.S. Munawar, Polyhedron **195**, 114988 (2021)
35. H. Kargar, R. Behjatmanesh-Ardakani, V. Torabi, A. Sarvian, Z. Kazemi, Z. Chavoshpour-Natanzi, V. Mirkhani, A. Sahraei, M.N. Tahir, M. Ashfaq, Inorg. Chim. Acta **514**, 120004 (2021)
36. H. Kargar, M. Ashfaq, M. Fallah-Mehrjardi, R. BehjatmaneshArdakani, K.S. Munawar, M.N. Tahir, J. Mol. Struct. **1253**, 132264 (2022)
37. H. Kargar, M. Ashfaq, M. Fallah-Mehrjardi, R. BehjatmaneshArdakani, K.S. Munawar, M.N. Tahir, J. Mol. Struct. **1261**, 132905 (2022)
38. G.M. Sheldrick, Acta Crystallogr., Sect. A **71**, 3 (2015)

39. G.M. Sheldrick, Acta Crystallogr. C **71**, 3 (2015)
40. A.L. Spek, Acta Crystallogr. D **65**, 148 (2009)
41 . C.F. Macrae, I. Sovago, S.J. Cottrell, P.T. Galek, P. McCabe, E. Pidcock, M. Platings, G.P. Shields, J.S. Stevens, M. Towler, J. Appl. Crystallogr. **53**, 226 (2020)
42. M.J. Frisch, G.W. Trucks, H.B. Schlegel, G.E. Scuseria, M.A. Robb, J.R. Cheeseman, G. Scalmani, etc. Gaussian 09 (Revision A.02), Gaussian, Inc., Wallingford, CT (2016).
43. http:// www. chemi ssian. com
44. R. Dennington, T.A. Keith, J.M. Millam, *GaussView (Version 6)* (Semichem Inc., Shawnee Mission, KS, 2016)
45. V. Dhayalan, M. Hayashi, Synthesis (2012). https:// doi. org/ 10. 1055/s- 0031- 12897 72
46. P.R. Spackman, M.J. Turner, J.J. McKinnon, S.K. Wolff, D.J. Grimwood, D. Jayatilaka, M.A. Spackman, J. Appl. Crystallogr. **54**, 1006 (2021)
47. M.A. Spackman, D. Jayatilaka, CrystEngComm **11**, 19 (2009) 48. A.R. Raza, S.L. Rubab, M. Ashfaq, Y. Altaf, M.N. Tahir, M.F. Rehman, T. Aziz, M. Alharbi, A.F. Alasmari, Molecules **28**, 5024 (2023)
49. J.J. McKinnon, D. Jayatilaka, M.A. Spackman, Chem. Commun. **37**, 3814 (2007)
50. A.N. Malik, M.N. Tahir, A. Ali, M. Ashfaq, M. Ibrahim, A.E. Kuznetsov, M.A. Assiri, M.Y. Sameeh, ACS Omega **8**, 25034 (2023)
51 . M.J. Turner, J.J. McKinnon, D. Jayatilaka, M.A. Spackman, CrystEngComm **13**, 1804 (2011)
52. S.L. Rubab, A.R. Raza, B. Nisar, M. Ashfaq, Y. Altaf, R. Hussain, N. Sajjad, M.S. Akram, M.N. Tahir, M.A. Shaheen, MFu. Rehman, H.M. Ali, Molecules **28**, 4375 (2023)
53. C. Tabares-Mendoza, P. Guadarrama, J. Organomet. Chem. **691**, 2978 (2006)
54. P. Geerlings, F. De Proft, W. Langenaeker, Chem. Rev. **103**, 1793 (2003)
55. N.V. Tzouras, S.P. Neofotistos, G.C. Vougioukalakis, ACS Omega **4**, 10279 (2019)
56 . Z. Demircioglu, Ç. Albayrak, O. Büyükgüngör, J. Mol. Struct. **1065–1066**, 210 (2014)
57. L. Wei, Y. She, Y. Yu, X. Yao, S. Zhang, J. Mol. Model. **18**, 2483 (2012)